Available online at www.sciencedirect.com

SciVerse ScienceDirect

journal homepage: www.elsevier.com/locate/he

Effect of hydrogen and syngas addition on the ignition of iso-octane/air mixtures

*Sudhanshu Jain, Dongru Li, Suresh K. Aggarwal**

Mechanical and Industrial Engineering, University of Illinois at Chicago, 842 W. Taylor Street, Chicago, IL 60607, USA

ARTICLE INFO

Article history:
Received 13 September 2012
Received in revised form
1 January 2013
Accepted 5 January 2013
Available online 18 February 2013

Keywords:
Hydrogen/iso-octane blends
Syngas/iso-octane blends
Ignition
Reaction pathways
Engine conditions

ABSTRACT

There is worldwide interest in using renewable fuels within the existing infrastructure. Hydrogen and syngas have shown significant potential as renewable fuels, which can be produced from a variety of biomass sources, and used in various transportation and power generation systems, especially as blends with hydrocarbon fuels. In the present study, a reduced mechanism containing 38 species and 74 reactions is developed to examine the ignition behavior of iso-octane/H_2 and iso-octane/syngas blends at engine relevant conditions. The mechanism is extensively validated using the shock tube and RCM ignition data, as well as three detailed mechanisms, for iso-octane/air, H_2/air and syngas/air mixtures. Simulations are performed to characterize the effects of H_2 and syngas on the ignition of iso-octane/air mixtures using the closed homogenous reactor model in CHEMKIN software. The effect of H_2 (or syngas) is found to be small for blends containing less than 50% H_2 (or syngas) by volume. However, for H_2 mole fractions above 50%, it increases and decreases the ignition delay at low ($T < 900$ K) and high temperatures ($T > 1000$ K), respectively. For H_2 fractions above 80%, the ignition is influenced more strongly by H_2 chemistry rather than by i-C_8H_{18} chemistry, and does not exhibit the NTC behavior. Nevertheless, the addition of a relatively small amount of i-C_8H_{18} (a low cetane number fuel) can significantly enhance the ignitability of H_2-air mixtures at NTC temperatures, which are relevant for HCCI and PCCI dual fuel engines. The CO addition seems to have a negligible effect on the ignition of i-C_8H_{18}/H_2/air mixtures, indicating that the ignition of i-C_8H_{18}/syngas blends is essentially determined by i-C_8H_{18} and H_2 oxidation chemistries. The sensitivity and reaction path analysis indicates that i-C_8H_{18} oxidation is initiated with the production of alkyl radical by H abstraction through reaction: i-$C_8H_{18} + O_2 = C_8H_{17} + HO_2$. Subsequently, the ignition chemistry in the NTC region is characterized by a competition between two paths represented by reactions R2 ($C_8H_{17} + O_2 = C_8H_{17}O_2$) and R8 ($C_8H_{17} + O_2 = C_8H_{16} + HO_2$), with the R8 path dominating, and increasing the ignition delay. As the amount of H_2 in the blend becomes significant, it opens up another path for the consumption of OH through reaction R36 ($H_2 + OH = H_2O + H$), which slows down the ignition process. However, for $T > 1100$ K, the presence of H_2 decreases ignition delay primarily due to reactions R31 ($O_2 + H = OH + O$) and R35 ($H_2O_2 + M = OH + OH + M$).

* *Corresponding author*. Tel.: +1 312 996 2235; fax: +1 312 413 0447.
E-mail address: ska@uic.edu (S.K. Aggarwal).

0360-3199/$ – see front matter
http://dx.doi.org/10.1016/j.ijhydene.2013.01.027

1. Introduction

Environmental concerns and desire to reduce dependency on fossil fuels have accelerated efforts to develop renewable and cleaner fuels for transportation and power generation. In this context, hydrogen (H_2) and syngas (primarily a mixture of H_2 and CO) are considered as a promising option for supplementing the use of conventional hydrocarbon fuels. Both of these fuels can be produced from a variety of renewable resources [1,2] and thus offer a virtually limitless supply.

Hydrogen has many desirable combustion characteristics including wider flammability limits and high burning velocities. The extended lean flammability limit offers significant advantages in reducing NO_x and soot emissions from practical combustors by reducing peak temperatures using leaner mixtures or dilution, such as exhaust gas recirculation (EGR) in IC engines. Similarly, the use of H_2 in gas turbine combustors can improve their lean blowout and emissions characteristics. Hydrogen also has a high autoignition temperature, which coupled with its high flame speed and diffusivity, can provide good antiknock properties, improve charge homogeneity, and reduce cycle-to-cycle variation in spark–ignition (SI) engines. In spite of these advantages, the development of hydrogen-powered IC (H_2ICE) on a commercial scale has faced many challenges due to storage and safety issues associated with H_2, and its low volumetric energy content. There are also technical challenges due to an increased propensity to preignite hydrogen–air mixtures and higher NO_x production due to high temperatures [3–5] at high engine loads.

A blended fuel strategy using a mixture of fossil fuel and H_2 (or fossil fuel and syngas) can address many of the above challenges. Moreover, such blends can be readily used within the existing infrastructure, and reduce greenhouse gas and other emissions associated with fossil fuels. Consequently, there have been numerous studies dealing with the ignition, combustion, and emission characteristics of H_2-hydrocarbon mixtures. Both fundamental and practical aspects of using such blends for transportation and power generation have been investigated. Fundamental studies have focused on CH_4/H_2 blends, and examined the effect of H_2 addition on flammability limits [6], laminar [7,8] and turbulent burning velocities [9], NO_x emissions [10–12], flame propagation characteristics including flame speed-stretch interactions [8,13], flame stability [14], and lean blowout limits [15]. There have also been engine studies on using various blends in compression ignition (CI) [16] and SI engines. Research dealing with SI engines has considered blends of H_2 with methane [17,18], natural gas [19–22], CNG [23], gasoline [22,24–28], biogas [29], methanol [30], and ethanol fuels [31]. An important result from these studies is that H_2 addition can generally provide noticeable improvement in engine performance in terms of combustion efficiency, increased burn rate, reduced cycle-to-cycle variations, and reduced CO, HC, and soot emissions. While this research has provided a wealth of information, it has also underlined the need for further studies on engine optimization, since the actual benefits would depend on a number of factors, such as compression ratio, overall equivalence ratio, engine speed, load, spark timing, and amount of H_2 in the blend. There is also a lack of fundamental information on the effects of H_2 on the combustion and emission behavior of gasoline and surrogate fuels.

This paper reports a numerical investigation on the ignition of iso-octane/H_2 and iso-octane/syngas blends at engine relevant conditions. The study is motivated by the growing interest in the use of renewable fuels, such as H_2 and syngas, in IC engines. The ignition characteristics of such blends are particularly important for their potential in improving the performance of HCCI (Homogeneous Charge Compression Ignition) and PCCI (Premixed Charge Compression Ignition) engines. For instance, the addition of H_2 or syngas can provide an effective strategy for controlling the ignition event and expanding the operation range of HCCI combustion in terms of equivalence ratio and engine load. Such studies are also important from fundamental aspects, as previous research has mostly focused on the ignition of CH_4/H_2 blends. Zhang et al. [32] and Huang et al. [33] reported shock tube data, while Levinsky et al. [34] reported rapid compression machine (RCM) data on the ignition of CH_4/H_2 blends for a range of pressures, temperatures, and blend compositions. The effect of H_2 was found to be negligible for blends containing less than 60% H_2 by volume, while the ignition behavior essentially resembled that of H_2 for blends containing more than 80% H_2. Aggarwal et al. [35] recently examined the effect of H_2 addition on the ignition of n-heptane, which is considered a primary reference fuel and a good surrogate for diesel. In this context, it is of interest to characterize the ignition behavior of iso-octane/H_2 blends, since iso-octane is also a primary reference fuel and surrogate for gasoline. Similarly it is important to study the ignition behavior of iso-octane/syngas blends due to the potential of using syngas in dual fuel engines [36,37].

The major objective of the present study is to develop a reduced kinetic mechanism and examine the ignition behavior of iso-octane/H_2 and iso-octane/syngas blends at engine relevant conditions. The kinetic model was developed by incorporating important H_2 and syngas oxidation reactions in an existing iso-octane skeletal mechanism [38]. The combined mechanism was validated using the available experimental data for the ignition of iso-octane-air [39,40], H_2-air, and syngas-air mixtures [41,42]. Further validation was performed through comparison with predictions using the comprehensive mechanisms for the oxidation of iso-octane [43,44], H_2 [45,46], and syngas [47]. A numerical study was then conducted to characterize the ignition behavior of iso-octane/H_2 and iso-octane/syngas blends. The sensitivity and reaction path analyses were also performed to identify the dominant reactions associated with the ignition of these blends, and to provide insight into the effects of H_2 and syngas on the ignition of iso-octane/air mixtures.

2. Physical numerical model

The physical model considers a reacting iso-octane/syngas/hydrogen/air mixture in a closed adiabatic system under constant volume conditions. Simulations were performed using the closed homogenous batch reactor model in CHEMKIN 10101. Note that the simulations under constant volume conditions have been shown to reproduce the shock tube and

rapid compression machine (RCM) experiments reasonably well. The numerical model uses an implicit time integration method to solve the transient stiff set of differential equations describing the mass, energy, and species conservations. As a starting point, the simulations considered the ignition of iso-octane-air mixtures using two mechanisms, namely the skeletal mechanism of Jia et al. [38] with 38 species and 69 gas phase reactions, and the detailed LLNL (Lawrence Livermore National Laboratory) mechanism [48] with 874 species and 3796 reactions. Computations were started with specified initial conditions, which include temperature, pressure, mixture composition and equivalence ratio (ϕ). As the radical species are produced following fuel oxidation, exothermic reactions are initiated and the mixture temperature increases. Consequently, the radical species concentrations increase, and the chemical activity is accelerated. The state of ignition was defined when the mixture temperature increases by 400 K with respect to initial temperature during simulations. Using other ignition criteria, such as one based on OH radical mole fraction, yielded essentially the same ignition delay time. Results are discussed in the next section.

3. Results and discussion

3.1. *Development of reduced mechanism for iso-octane/H_2/CO blends*

The starting point in the development of the reduced mechanism was the Jia et al. skeletal mechanism [38], which has been optimized against ignition delay data under engine relevant conditions. We performed further validation for this mechanism using the detailed LLNL mechanism [48], and the shock tube and RCM ignition data for iso-octane/air mixtures. Fig. 1 compares the predicted ignition delay times using these two mechanisms with the shock tube ignition data [39] at $\phi = 0.5$ and 1.0. Note that the experimental data has been normalized with respect to a pressure of 50 atm. As indicated in Fig. 1, the Jia et al. mechanism exhibits reasonably good agreement with both the measurements and the predictions of the LLNL mechanism. In particular, it captures the NTC behavior characterized by the drop in ignition delay as the initial temperature is reduced. Compared to the LLNL mechanism, the reduced mechanism indicates a slightly higher rolloff temperature and a more severe rolloff. Fig. 2 presents the corresponding comparison with the RCM data [40] at $\phi = 0.4$. Again, there is good agreement between predictions and measurements, although both the mechanisms underpredict ignition delays compared to experiments at higher temperatures.

While the Jia et al. mechanism was able to reproduce the experimentally observed ignition behavior for iso-octane/air mixtures, it required modifications for predicting the ignition delays for H_2/air and syngas/air mixtures. Conaire et al. [45] mechanism and Davis et al. [47] mechanism were used to identify the most important reactions associated with the ignition of H_2/air and syngas/air mixtures, respectively. Sensitivity analysis with respect to the ignition delay was performed using these mechanisms. The normalized sensitivity with respect to a given reaction is defined as

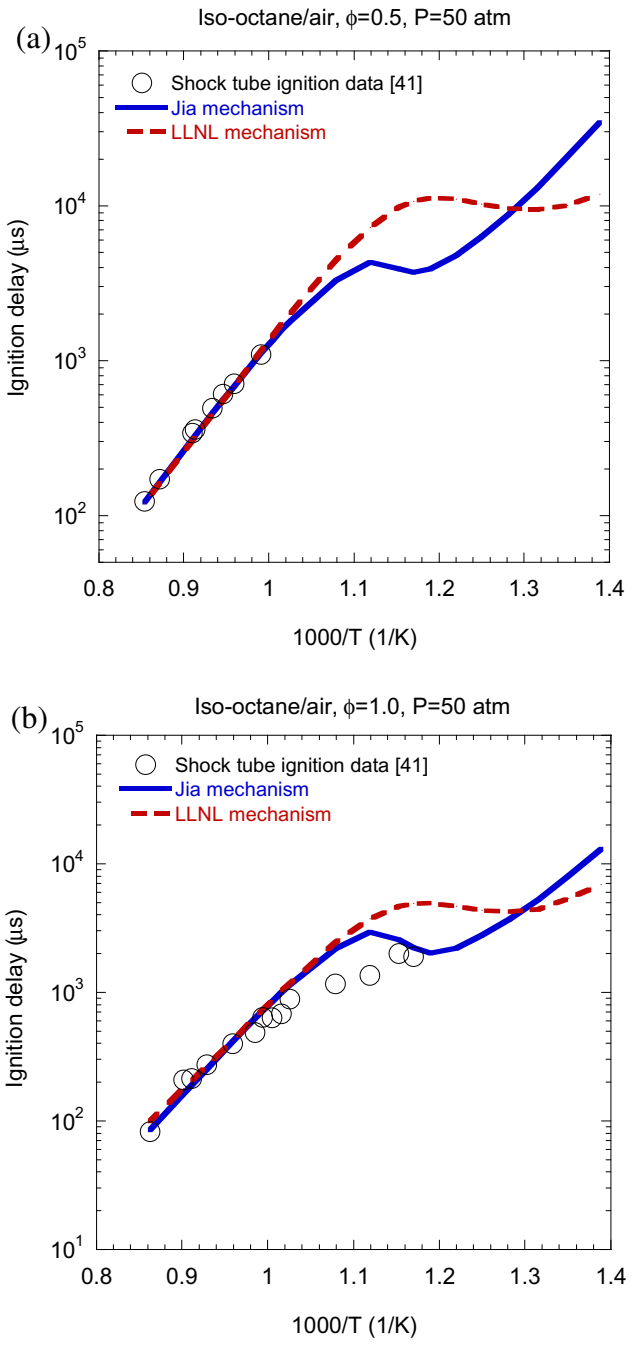

Fig. 1 – Predicted and measured ignition delay times for iso-octane/air mixtures at equivalence ratio $\phi = 0.5$ (a) and $\phi = 1.0$ (b). Predictions are based on Jia et al. mechanism (solid line) and the detailed LLNL mechanism (dashed line), while shock tube measurements (open circle), normalized to a pressure of 50 atm, are from Davidson et al. [39].

$$S = \frac{\partial \ln \tau}{\partial \ln k} = \frac{k}{\tau}\frac{\partial \tau}{\partial k} \quad (1)$$

Here τ is the predicted ignition delay and k is the rate constant of reaction under consideration. The value of S was determined by calculating the change in ignition delay time after doubling the reaction rate constant. Then Eqn. (1) reduces to

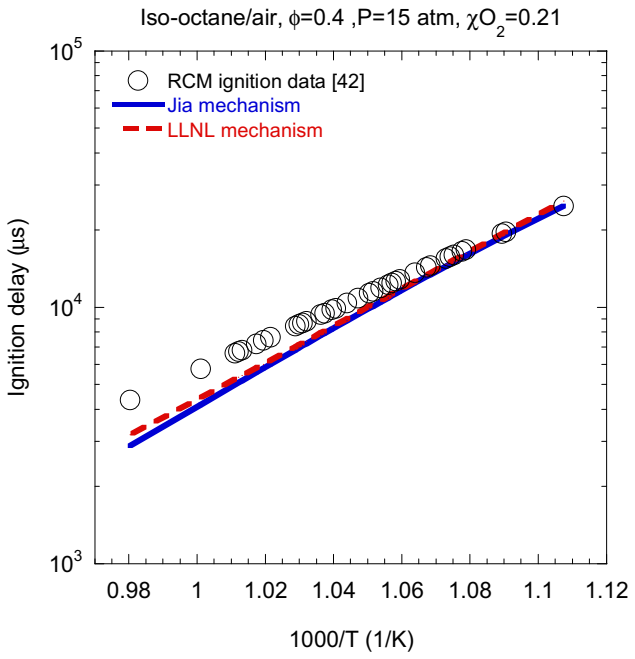

Fig. 2 – Predicted and measured ignition delay times for iso-octane/air mixtures. Predictions are based on Jia et al. mechanism (solid line) and the detailed LLNL mechanism (dashed line), and the normalized RCM ignition data is from Walton et al. [40].

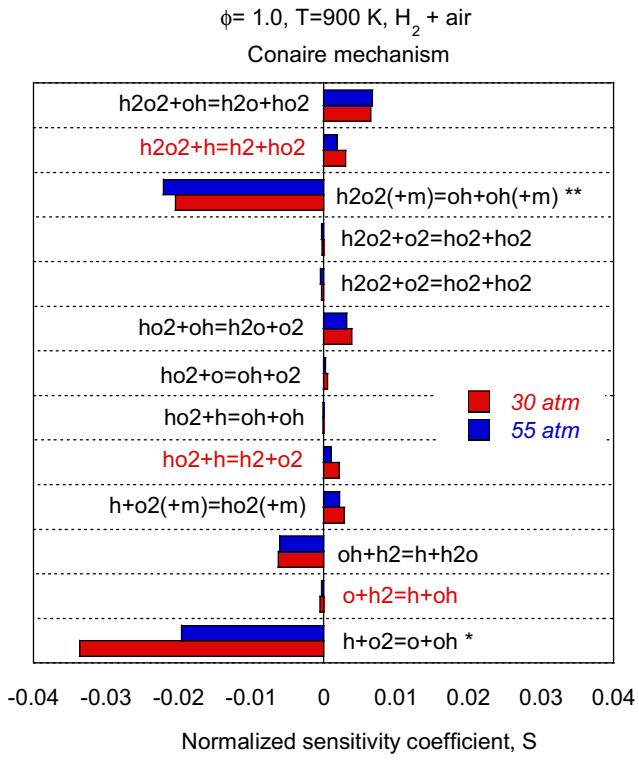

Fig. 3 – Normalized sensitivity coefficient for H_2/air mixtures at 30 atm and 55 atm, $T = 900$ K and $\phi = 1.0$. Simulations are based on the Conaire mechanism. *Plotted to 1/10th scale. **Plotted to 1/2 scale.

$$s = \frac{(\tau(2k) - \tau(k))}{\tau(k)} \quad (2)$$

Thus a negative value of S implies reduction in ignition delay as the reaction rate constant (k) is increased. Note that for a given reaction, both the forward and backward reaction rate constants were multiplied by a factor of 2. Fig. 3 shows the computed values of S for the most important reactions associated with the ignition of H_2/air mixtures at two different pressures, and temperature $T = 900$ K. Among the key reactions identified above, the following three reactions were added to the Jia et al. mechanism.

$$O + H_2 = H + OH \quad (R70)$$

$$HO_2 + H = H_2 + O_2 \quad (R71)$$

$$H_2O_2 + H = H_2 + HO_2 \quad (R72)$$

Other reactions shown in Fig. 3 were already present in the mechanism. Since this mechanism contains 69 reactions, the three reactions added are numbered after 69. These three reactions are shown in red color in Fig. 3. Reactions R70 and R71 are the important initiation reactions for H_2 oxidation, while the reverse reaction of R71 is necessary to initiate the reaction between H_2 and O_2. Another key reaction is R72, which becomes active at high temperatures in the reverse direction, and produces H_2O_2 that subsequently OH radicals through R35, and thus enhances ignition. The sensitivity analysis performed at other temperatures and equivalence ratios identified the same key reactions as indicated in Fig. 3.

A similar sensitivity analysis was performed for the ignition of syngas/air mixtures using the Davis mechanism [47]. Fig. 4 shows the normalized sensitivity coefficients with respect to the important reactions for the ignition of 50/50 H_2/CO (by volume) blend. Other conditions are the same as those in Fig. 3 with $T = 900$ K and $\phi = 1.0$. As indicated in Figs. 3 and 4, the key reactions pertaining to H_2 oxidation are the same in the two mechanisms. Among the reactions shown in Fig. 4, the following two reactions pertaining to CO oxidation (shown in red color) were added to the Jia mechanism:

$$CO + O_2 = CO_2 + O \quad (R73)$$

$$CO + HO_2 = CO_2 + OH \quad (R74)$$

Both of these reactions supplement the reaction R28 in converting CO to CO_2. The sensitivity analysis at a higher temperature (1400 K) revealed two other important reactions for CO oxidation:

$$CO + OH = CO_2 + H \quad (R28)$$

$$HCO + M = H + CO + M \quad (R41)$$

However, these reactions were already present in the Jia mechanism. Thus our modified reduced mechanism contained 74 reactions with five additional reactions added to the Jia mechanism.

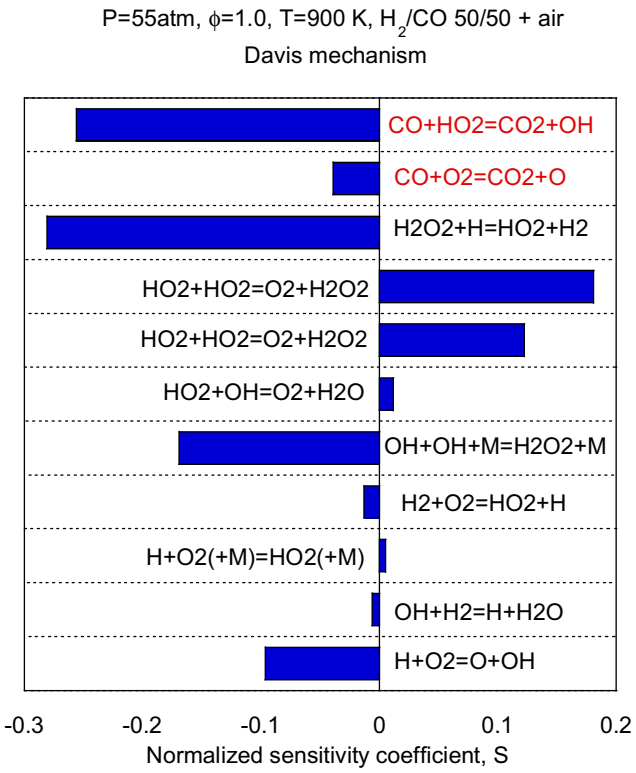

Fig. 4 – Normalized sensitivity coefficient for syngas/air mixture with 50/50 H_2/CO blend at 55 atm, $T = 900$ K and $\phi = 1.0$. Simulations are based on the Davis mechanism [47].

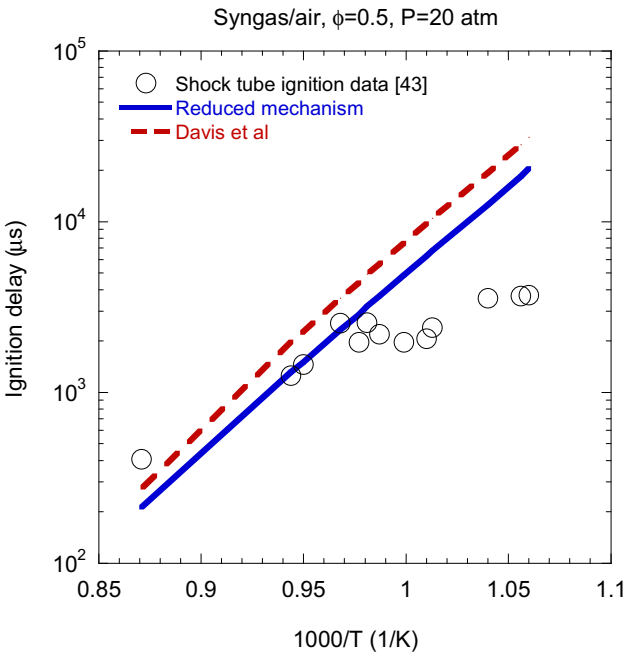

Fig. 5 – Predicted ignition delay for syngas compared with shock tube experimental data [41] (open circles). Predictions are based on our reduced mechanism (solid line) and Davis et al. [47] mechanism (dashed line). Experimental data has been normalized to 20 atm.

3.2. *Validation of the reduced mechanism*

The modified reduced mechanism was validated against the available shock tube and RCM ignition data. Figs. 5 and 6 compare the predicted ignition delays for syngas/air mixtures with the shock tube [41] and RCM data [42], respectively. The predictions using the Davis mechanism [47] are also shown. As noted in these figures, the measured values are normalized with respect to a specific pressure. There is good agreement between the predictions and measurements for temperatures above 1000 K. However, for temperatures below 1000 K, there are significant discrepancies between the predictions and experimental data. Similar discrepancies at low temperatures have been observed in previous studies [41,49], and attributed to mixture non-homogeneities present in RCM experiments, but are not duplicated in simulations. In particular Dryer et al. [49] stated "ignition delay measurements in the mild ignition regime are strongly susceptible to perturbations and that model predictions of ignition delays that do not account for these perturbations can be significantly misleading".

Figs. 5 and 6 further indicate that our reduced mechanism underpredicts the ignition delay compared to the Davis mechanism. Further analysis indicated that this is primarily due to the differences in the rate constants for reaction R35 for the dissociation of hydrogen peroxide:

$$H_2O_2 + M = OH + OH + M \qquad (R35)$$

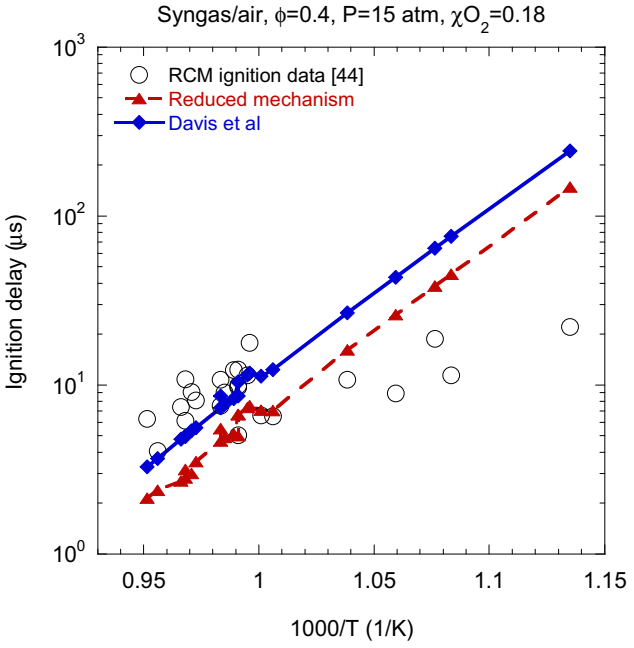

Fig. 6 – Predicted ignition delays for syngas/air mixtures compared with normalized RCM ignition data [42] (open circles). Predictions are based on our reduced mechanism (diamonds) and Davis et al. [47] mechanism (triangles). Experimental data is normalized to a pressure of 15 atm.

The rate constants used in our reduced mechanism were taken from the skeletal mechanism of Patel et al. [50], who optimized the rate constants for high pressures conditions using data from HCCI experiments. The rate constants in the Davis mechanism were based on several studies cited in Ref. [47], which considered pressure dependency through Troe fall-off formula [32]. It is also important to note that one could easily improve the agreement for the ignition of H_2-air mixtures by adjusting the above rate constants. However, this may affect the prediction of ignition delays for i-C_8H_{18}/syngas blends, since the rate constants have been optimized for these blends.

3.3. *Analysis of the NTC region*

An important criterion for validating a given mechanism especially for engine relevant conditions is that it should capture the NTC chemistry associated with the ignition of large hydrocarbon fuel species. While the reduced mechanism has been shown to reproduce the NTC behavior, this aspect is further examined through a reaction pathway and sensitivity analysis. Consistent with previous studies [43,44], the analysis indicated that the fuel oxidation is initiated by H abstraction and production of alkyl radical through reaction R1

$$iC_8H_{18} + O_2 = C_8H_{17} + HO_2 \quad \text{(R1)}$$

Subsequently, the ignition chemistry is characterized by two competing paths depending upon the temperature. The first path involves the production of alkylhydroperoxyradical through reactions R2 and R3, which then reacts with O_2 to form peroxy-alkylhydroperoxy radical. The latter species readily decomposes to form ketohydroperoxide through reaction R5, which then decomposes to form additional OH through reaction R6. This produces sufficient OH radical pool to accelerate the exothermic reactions and the ignition process, as indicated by reaction R7 that produces alkyl radical to feed into the above chain (R2–R7).

$$C_8H_{17} + O_2 = C_8H_{17}O_2 \quad \text{(R2)}$$

$$C_8H_{17}OO = C_8H_{16}OOH \quad \text{(R3)}$$

$$C_8H_{16}OOH + O_2 = OOC_8H_{16}OOH \quad \text{(R4)}$$

$$OOC_8H_{16}OOH = OC_8H_{15}OOH + OH \quad \text{(R5)}$$

$$OC_8H_{15}OOH = OC_8H_{15}O + OH \quad \text{(R6)}$$

$$iC_8H_{18} + OH = C_8H_{17} + H_2O \quad \text{(R7)}$$

This path dominates the fuel oxidation chemistry at low temperatures. At higher temperatures, i.e., in the NTC region, the competing path through reaction R8 becomes more active. This has the effect of slowing down the ignition process, as it leads to the formation of H_2O_2 through reaction R37, which is known to be a metastable species at temperatures corresponding to the NTC regime and lower.

$$C_8H_{17} + O_2 = C_8H_{16} + HO_2 \quad \text{(R8)}$$

$$HO_2 + HO_2 = H_2O_2 + O_2 \quad \text{(R37)}$$

The relative contribution of each of these two paths is illustrated in Fig. 7, which plots the rate of production (ROP) or the O_2 consumption rate for reactions R2 and R8 at different temperatures. At $T = 700$ K, the O_2 consumption rate due to R2 is higher than that due to R8, while at $T = 800$ K, which is in NTC regime, the two rates become comparable. At still higher temperatures, $T = 900$ K and 1000 K, the O_2 consumption rate due to R8 significantly exceeds that due to R2, indicating the slowing down of the first reaction path represented by R2–R7. As temperature is increased further, i.e. above the NTC regime, the reaction R35 becomes active producing significant amount of OH radicals and accelerating the ignition process.

$$H_2O_2 + M = OH + OH + M \quad \text{(R35)}$$

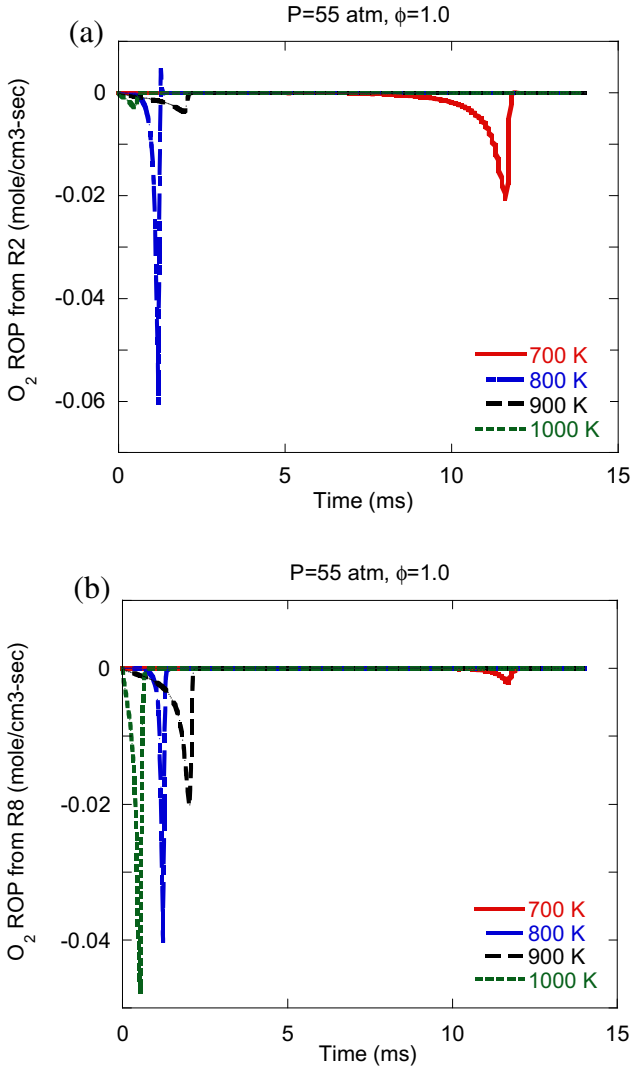

Fig. 7 – Rate of production of O_2 due to reactions R2 (Fig. a) and R8 (Fig. b) at different initial temperatures. Simulations are done using our reduced mechanism at pressure 55 atm and $\phi = 1.0$.

The relative importance of reactions R2 and R8 was further assessed by computing the normalized sensitivity coefficient using Eq. (2). Fig. 8 shows the normalized sensitivity coefficients for reactions R2 and R8 at different initial temperatures. As expected, the sensitivity coefficients for R2 and R8 have negative and positive values, respectively. The sensitivity coefficient for R8 has its highest values in the NTC regime, i.e., between 800 and 900 K. Moreover, its value far exceeds that of R2, indicating that it noticeably slows down the ignition process in this regime. Fig. 9 presents the normalized sensitivity coefficients for reactions R35 and R37. For temperatures above 700 K, both of these reactions promote ignition. As discussed earlier, R37 produces H_2O_2, which is metastable species at lower temperatures, but becomes increasingly active at temperatures above 900 K, providing OH radicals through reaction R35 and accelerating the ignition process. This is clearly illustrated in Fig. 9. Thus, the above results clearly demonstrate the capability of the reduced mechanism to capture the dominant reaction pathways characterizing the ignition process in the NTC region.

The ability of the reduced mechanism to predict the ignition behavior of i-C_8H_{18}/H_2 blends was further assessed by comparing its predictions with those using the Conaire mechanism [45] and LLNL mechanism [48] for the ignition of H_2/air mixtures. Note that the Conaire mechanism for H_2 oxidation has been extensively validated using a variety of targets. Results for the ignition of H_2/air mixture at $\phi = 1$, $p = 55$ atm are presented in Fig. 10, and clearly demonstrate the ability of the reduced mechanism to capture the H_2 ignition chemistry under engine relevant conditions. Having validated our reduced mechanism against the ignition data for iso-octane/air, syngas/air, and H_2/air mixtures, results now focus on the effects of H_2 and syngas addition on the ignition behavior of iso-octane/air mixtures.

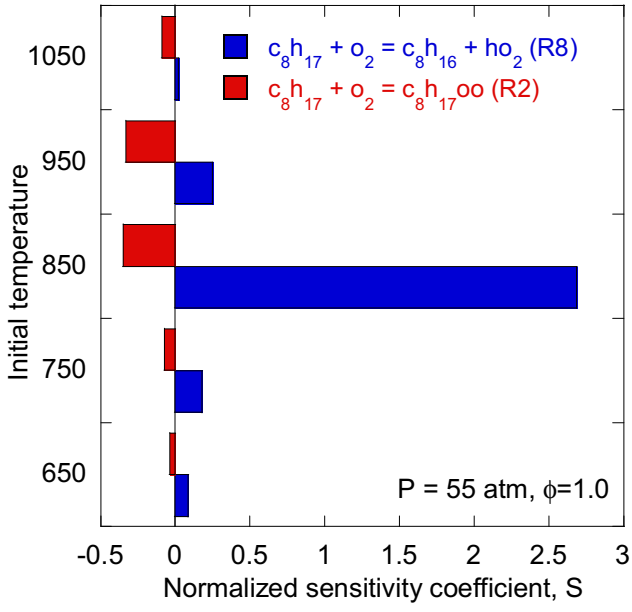

Fig. 8 – Normalized sensitivity coefficients for reactions R2 and R8 calculated at different initial temperatures using Eq. (2) for iso-octane/air mixture. Simulations are done using our reduced mechanism.

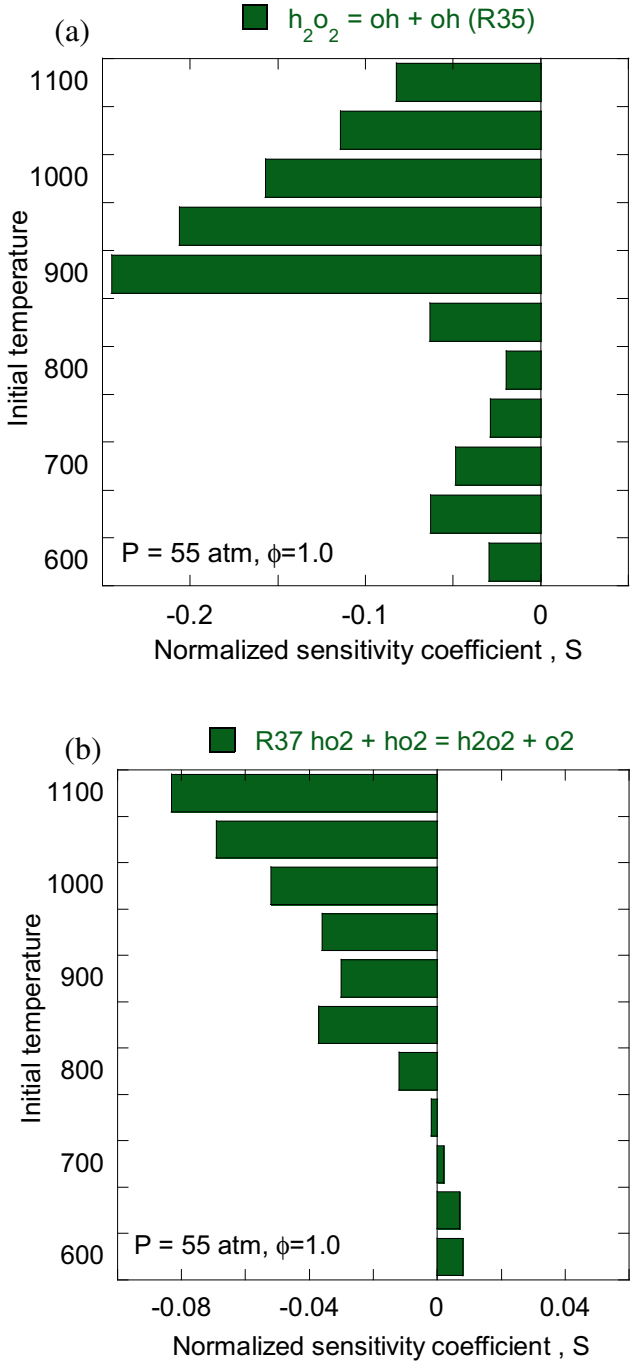

Fig. 9 – Normalized sensitivity coefficients with respect to reactions R35 (Fig. a) and R37 (Fig. b) calculated at different initial temperatures for iso-octane/air mixtures. Simulations are based on our reduced mechanism.

3.4. *Effect of H_2 on the ignition of i-C_8H_{18}/air mixtures*

Fig. 11 presents the effect of H_2 addition on the ignition of i-C_8H_{18}/air mixtures using our reduced mechanism and LLNL

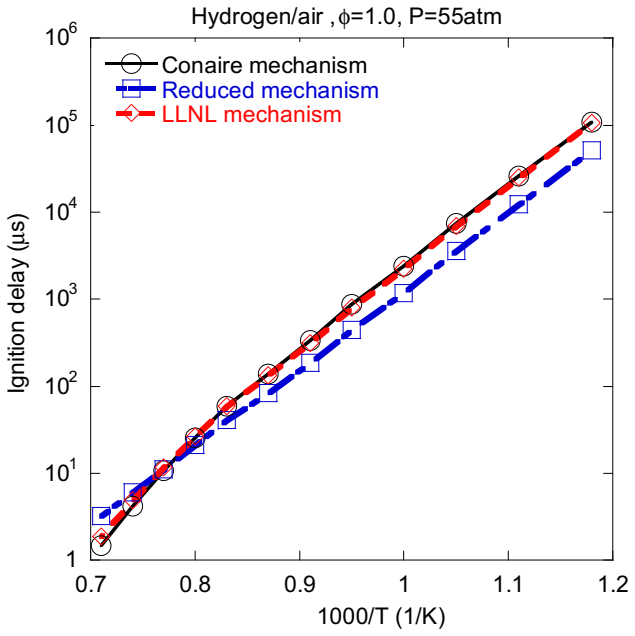

Fig. 10 – Predicted ignition delay times for H_2/air mixture using our reduced mechanism (square), Conaire et al. [45] mechanism (circle), and LLNL mechanism (diamond).

mechanism. Results are presented in terms of the plot of ignition delay time as a function of initial temperature for different i-C_8H_{18}/H_2 blends at pressure $p = 55$ atm. Results for the reduced mechanism are shown for $\phi = 0.7$, $\phi = 1$ and $\phi = 2$, while those for the LLNL mechanism are shown for $\phi = 1$ (Fig. 11d). There is reasonably good agreement between the ignition delay predictions of the two mechanisms, although there are some quantitative differences. The effect of H_2 appears to be somewhat less pronounced with the LLNL mechanism, especially at lower temperatures ($T < 900$ K). In general, for the both the mechanisms, the effect of H_2 addition is relatively small for H_2 fraction below 50%, but becomes increasingly significant for H_2 fraction above 50%. The overall effect of H_2 is to increase the ignition delay at low temperatures ($T < 900$ K), and decrease it at high temperatures ($T > 1000$ K). As the H_2 fraction exceeds 80%, the ignition behavior is more strongly influenced by the H_2 oxidation chemistry. For instance, for such blends, the ignition delay plots do not exhibit the NTC behavior. Another way to interpret these results is that the presence of a relatively small amount of i-C_8H_{18} (a low cetane number fuel) can significantly enhance the ignitability of H_2-air mixtures at temperatures below 1000 K. This temperature range is important for HCCI and PCCI dual fuel engines.

It is important to note that further comparison of results obtained using our reduced model and the detailed LLNL model indicated noticeable differences in the ignition delay predictions at low temperatures ($T < 800$ K), and for blends with H_2 fraction between 70 and 90%. For these conditions, the reduced mechanism considerably overpredicts ignition delays compared to the detailed mechanism. To investigate this behavior, we performed sensitivity analysis for the two mechanisms for a blend with 80% H_2, and at 700 K and 55 atm. The sensitivity analysis with reduced mechanism identified two dominant reactions, R7 (i-C_8H_{18} + OH = C_8H_{17} + H_2O) and R36 (H_2 + OH = H_2O + H), affecting the ignition delay. The corresponding analysis with LLNL mechanism identified essentially the same two reactions affecting the ignition delay. While the dependence of the reaction rate constant (k) on temperature for reaction R36 was essentially the same in the two mechanisms, that for reaction R7 was noticeably different. The difference was due to the production of four alkyl radical (C_8H_{17}) isomers for reaction R7 in the detailed mechanism, as indicated below:

Reaction# (detailed mechanism)		A	b	E
(R3373)	i-C_8H_{18} + OH<=>AC_8H_{17} + H_2O	2.63E + 07	1.8	1431.0
(R3374)	i-C_8H_{18} + OH<=>BC_8H_{17} + H_2O	9.00E + 05	2.0	−1133.0
(R3375)	i-C_8H_{18} + OH<=>CC_8H_{17} + H_2O	1.70E + 06	1.9	−1450.0
(R3376)	i-C_8H_{18} + OH<=>DC_8H_{17} + H_2O	1.78E + 07	1.8	1431.0

Symbols A, b, and E are parameters in the reaction rate constant, $k = A\,T^{**}b\,\exp(-E/RT)$. The four alkyl isomers further react to produce more OH radicals and thus accelerate the ignition process for the detailed mechanism. Since the reduced mechanism does not contain these isomers, all the above four reactions correspond to reaction R7 in this mechanism. In order to account for the effect of isomers, the reaction rate constant of R7 in the reduced mechanism was increased by a factor of 4, and the results are shown in Fig. 12, which plots ignition delays for a blend with 80% H_2. With the modified reaction rate for R7, we were able to match the ignition delay predictions of reduced mechanism with those of detailed mechanism at low temperatures, as clearly indicated in the figure. Moreover, ignition delay predictions using the modified R7 reaction rate in the reduced mechanism were not noticeably affected at other conditions.

3.5. *Effect of syngas on the ignition of i-C_8H_{18}/air mixtures*

Since syngas primarily contains H_2 and CO, its effect can be characterized in terms of the effect of CO addition on the ignition of i-C_8H_{18}/air mixtures. Fig. 13 presents the ignition delays computed using the reduced mechanism (Fig. 13a) and LLNL mechanism (Fig. 13b) for different i-C_8H_{18}/CO blends at $p = 55$ atm and $\phi = 1.0$. The addition of CO seems to have a negligible effect on the ignition of i-C_8H_{18}/air mixtures, except at low temperatures ($T < 900$ K) and for blends containing more than 90% CO by volume. Under latter conditions, the CO addition increases the ignition delay. However, it is difficult to envision using hydrocarbon-syngas blends with such large CO fractions, since the current research and development efforts are directed toward using hydrogen rich syngas through various carbon capture technologies. Thus an important result here is that the ignition behavior of i-C_8H_{18}/syngas blends is largely dominated by the i-C_8H_{18} and H_2 oxidation chemistries.

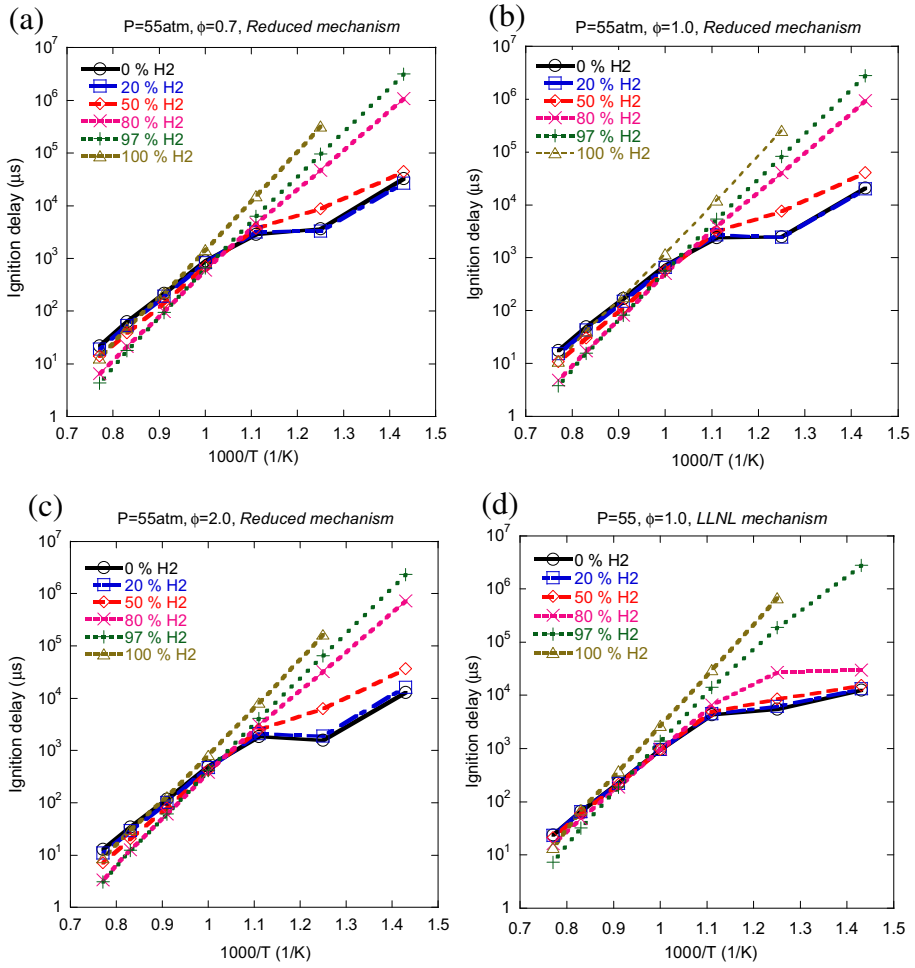

Fig. 11 – Predicted ignition delay times for iC_8H_{18}–H_2 blends with different amounts of H_2 (by volume) in the blend. Results for the reduced mechanism are shown for $\phi = 0.7$ (Fig. a), $\phi = 1.0$ (Fig. b), $\phi = 2.0$, (Fig. c), while those for the LLNL mechanism are shown for $\phi = 1.0$ (Fig. d). Pressure is 55 atm.

3.6. *Sensitivity and reaction path analysis*

The sensitivity and reaction path analysis were performed to gain further insight into the effect of H_2 on the ignition of i-C_8H_{18}/air mixtures. Fig. 14 plots the normalized sensitivity coefficient with respect to various reactions for i-C_8H_{18}/H_2 blends containing 0% and 80% H_2 by volume. Results for $T = 820$ K and 880 K are presented to highlight the NTC region, while those for $T = 1100$ K are to characterize the high temperature ignition chemistry. As discussed earlier, for the 0% H_2 case, the ignition chemistry in the NTC region is characterized by competition between the two oxidation paths represented by reactions R2 and R8, with the R8 path dominating and increasing the ignition delay. This is clearly illustrated by the sensitivity coefficient plot in Fig. 14a. At higher temperatures ($T = 1100$ K), however, the important reactions affecting ignition are R1, R35, R37, and R49. Reactions R1, R35, R37 have been discussed in an earlier section, and, as expected, promote ignition. Reaction R49 ($HO_2 + OH = H_2O + O_2$) consumes radical species and thus increases the ignition delay.

For the 80% H_2 case, the presence of H_2 increases ignition delay considerably in the NTC region, but decreases it in the high temperature region (cf. Fig. 11). The sensitivity results in Fig. 14 indicate that the increase in ignition delay in the NTC region is primarily caused by reaction R36 ($H_2 + OH = H_2O + H$), which consumes OH radicals that are being produced through reactions R5 and R6, and feed the reaction path represented by R2–R7, as part of the iso-octane oxidation chemistry discussed earlier. Thus the depletion of OH radical pool due to reaction R36 slows down the ignition process in the NTC region. Moreover, at high H_2 fraction in the blend, the role of NTC chemistry becomes less important. It also renders reactions R9 and R5, associated with iso-octane oxidation, less important in the NTC regime. At high temperatures ($T = 1100$ K), the effect of H_2 addition is to enhance the ignition process. This is due to the fact that the ignition behavior is increasingly influenced by the H_2 oxidation chemistry, as exemplified by reaction R31 ($O_2 + H = OH + O$) and R35, both of which decrease ignition delay (cf. Fig. 14b). In addition, reactions R32 ($HO_2 + H = OH + OH$) and R36 ($H_2 + OH = H_2O + H$) become important and reduce ignition

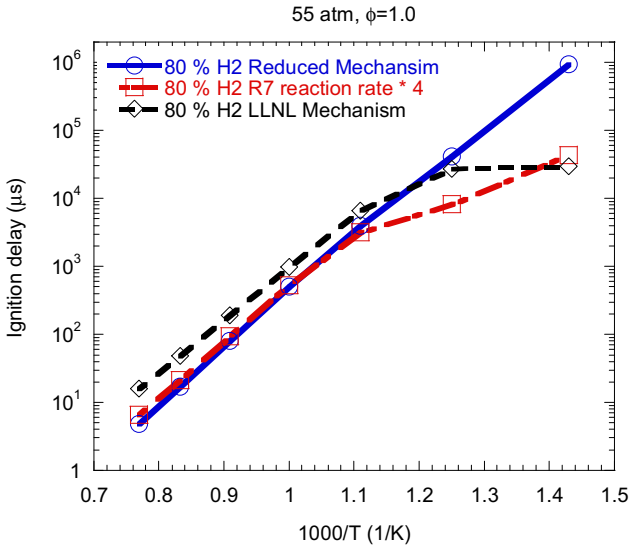

Fig. 12 – Predicted ignition delay times for i-C_8H_{18}–H_2 blend with 80% H_2. Results are shown for the LLNL mechanism (diamond), reduced mechanism (circle) and reduced mechanism with reaction R7 modified (square).

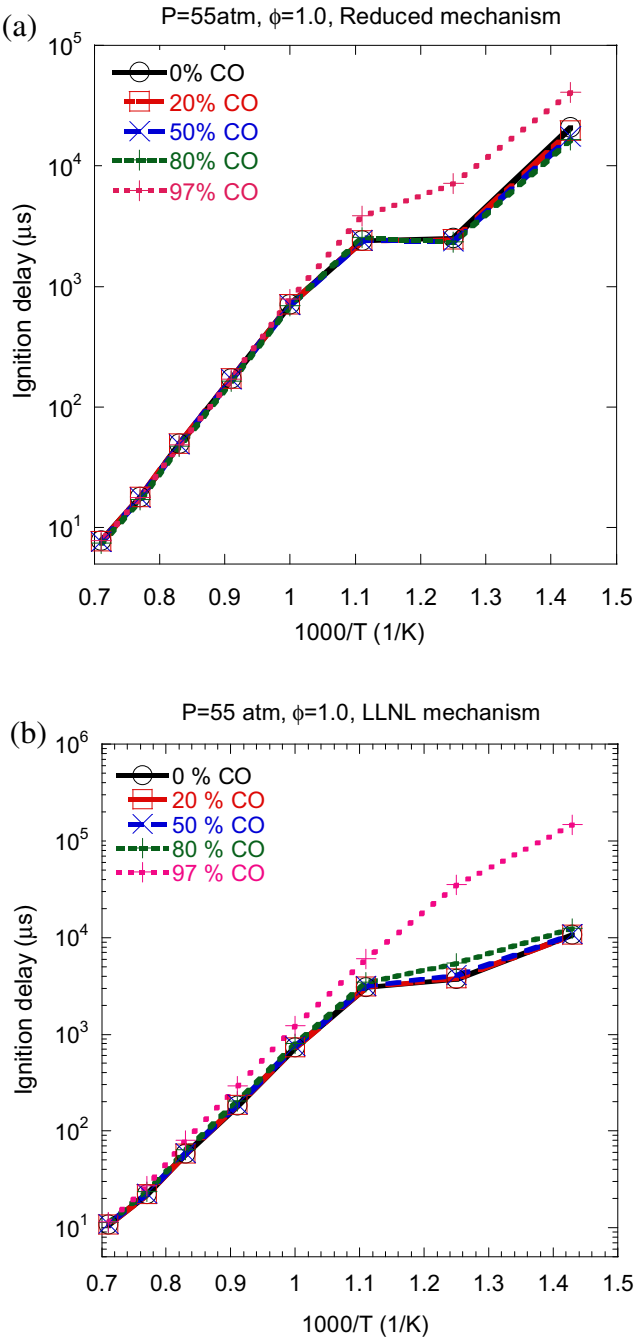

Fig. 13 – Predicted ignition delay time plotted for different iC_8H_{18}/CO blends at $p = 55$ atm and $\phi = 1.0$. Simulations were performed using the reduced mechanism (Fig. a) and the LLNL mechanism (Fig. b).

delay, but this effect is largely negated by reaction R34 ($H + O_2 + M = HO_2 + M$), which increases ignition delay.

Another useful way to interpret the ignition behavior of blends is that the addition of a relatively small amount i-C_8H_{18} can significantly affect the ignition of H_2/air mixtures. Thus, the presence of a low cetane number fuel, such as i-C_8H_{18}, can noticeably enhance the ignitability of H_2 in the NTC region. Results summarizing this aspect are presented in Fig. 15, which plots the normalized sensitivity coefficient with respect to various reactions for i-C_8H_{18}/H_2 blends with 0%, 3%, and 20% i-C_8H_{18} at $T = 820$ K and 1200 K. As indicated in Fig. 15a, the reduction in ignition delay in the NTC region is primarily due to the opening up of the i-C_8H_{18} oxidation route through reactions R1 and R7 as discussed earlier. As the i-C_8H_{18} mol fraction in the blend is increased, reaction R8 becomes more important and, consequently, the ignition behavior is increasingly influenced by the NTC chemistry. At high temperatures (cf. Fig. 15b), the increase in ignition delay due to i-C_8H_{18} addition is mainly caused by the fact that its oxidation route through reactions R1 and R7 as well as reaction R72, which promote ignition, become less important.

Fig. 16 presents the reaction path diagrams for the ignition of i-C_8H_{18}/H_2 blends with 0% H_2 (Fig. 16a) and 80% H_2 (Fig. 16b) at $p = 55$ atm, $T = 850$ K, $\phi = 1.0$, and time = 0.975 ms. Note that the ignition delay times for these cases are 1.82 ms and 12.025 ms, respectively. The '%' with each arrow indicates the percentage of a species being consumed by a given reaction; for example, in Figs. 16a and, 98.9% of i-C_8H_{18} is being consumed by reaction R7 to produce the alkyl radical, while only 40.4% of OH is consumed in this reaction. For both cases, the iso-octane oxidation starts with the production of alkyl radical by H abstraction through reaction R1, as discussed earlier in the context of NTC behavior. However, this reaction is not seen in Fig. 16a for the 0% H_2 case, but appears in Fig. 16b for the 80% H_2 case, since it is only significant early during the ignition process. Later during the ignition process, i-C_8H_{18} is mostly (98.9%) consumed through R7. The subsequent fuel oxidation then follows two competing paths, as discussed earlier. One involves the production of ketohydroperoxide, which decomposes to form OH, which then reacts with i-C_8H_{18} to produce alkyl radical to feed into this path, while the

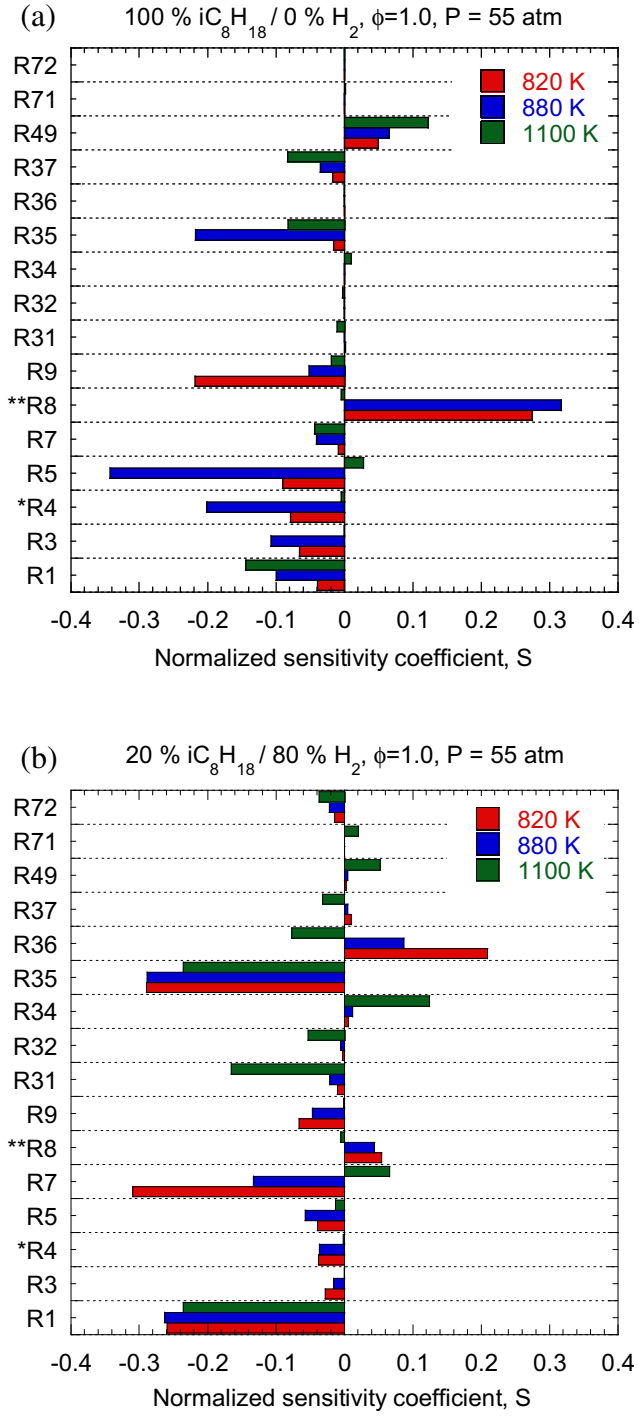

Fig. 14 – Normalized sensitivity coefficients calculated for 0% H_2 (Fig. a) and 80% H_2 (Fig. b) at three different temperatures. Simulations are based on our reduced mechanism. *Plotted to 1/2 scale. **Plotted to 1/4 scale.

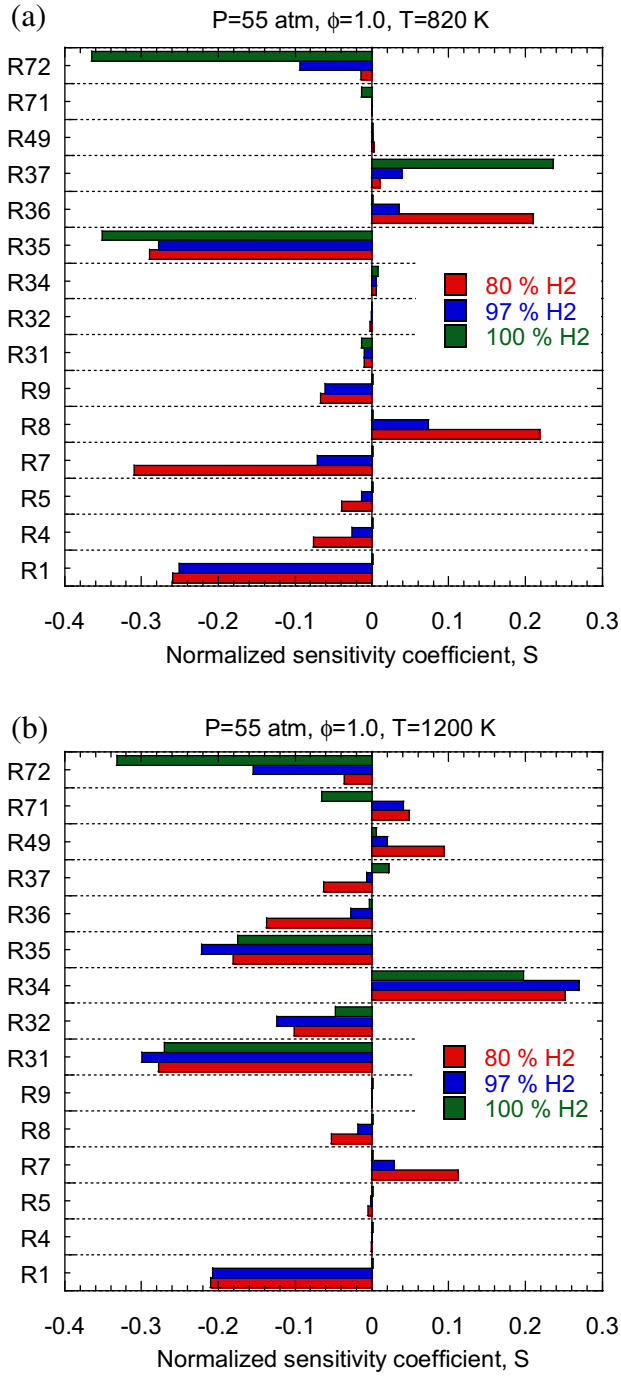

Fig. 15 – Normalized sensitivity coefficients calculated for 100% H_2, 97% H_2, and 80% H_2 in the iC_8H_{18}/H_2 blend at 820 K (Fig. a) and 1200 K (Fig. b). Simulations are based on the reduced mechanism.

second path involves the formation of C_8H_{16} and HO_2. Both of these paths are active in the 0% and 80% H_2 cases, as shown in Fig. 16. However, for the latter case, the presence of H_2 opens another path for the consumption of OH through reaction R36 (cf. Fig. 16b), which has the effect of slowing down the i-C_8H_{18} oxidation rate through its reaction with OH, and thus reducing the production of C_8H_{17}. For example, as indicated in Figs. 16 and 40.4% of OH consumption is used to produce alkyl radical (C_8H_{17}) in the 0%H_2 case compared to only 16.2% in the 80% H_2 case.

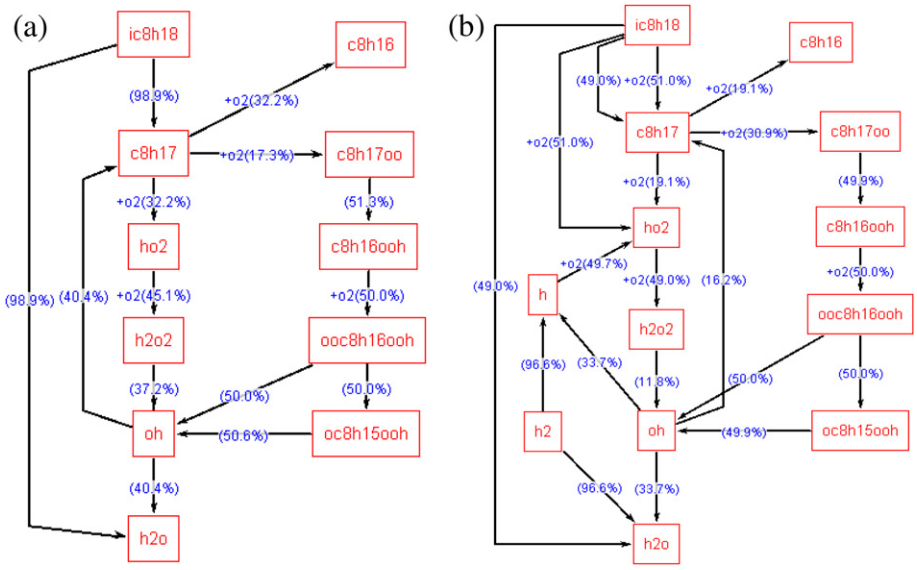

Fig. 16 – Reaction pathway analysis for two iC_8H_{18}/H_2 blends with 0% H_2 (Fig. a) and 80% H_2 (Fig. b). Other conditions are $p = 55$ atm, $T = 850$ K, $\phi = 1.0$ and time = 975 μs. Simulations are based on our reduced mechanism.

4. Conclusions

A reduced mechanism containing 38 species and 74 reactions has been developed to examine the ignition characteristics of iso-octane/H_2 and iso-octane/syngas blends at engine relevant conditions. The mechanism was validated using the shock tube and RCM ignition data for iso-octane/air, H_2/air and syngas/air mixtures. Further validation was performed by comparing its predictions with those using the LLNL detailed mechanism with 874 species and 3796 reactions for iso-octane, the Conaire mechanism with 10 species and 21 reactions for H_2, and the Davis mechanism consisting of 14 species and 38 reactions for syngas. The reduced mechanism was then used to characterize the effects of H_2 and syngas on the ignition of iso-octane/air mixtures in a closed homogenous reactor at temperatures between 700 and 1400 K, equivalence ratios between 0.5 and 2.0, and pressure of 55 atm. The sensitivity and reaction path analysis were also performed to gain further insight into the ignition behavior of blends. Important observations are:

1. The reduced mechanism shows good agreement with shock tube and RCM measurements for the ignition of iso-octane/air, H_2/air and syngas/air mixtures. It also reproduces the experimentally observed NTC regime for iso-octane/air mixtures. However, there are significant discrepancies between its predictions and RCM data for syngas/air mixtures at lower temperatures ($T < 1000$ K). Similar discrepancies have been observed by other researchers using the LLNL and the Davies mechanisms, and attributed to mixture non-homogeneities present in the RCM experiments, but are not duplicated in simulations.
2. There is good agreement between the predictions of the reduced mechanism and the three detailed mechanisms for the ignition of iso-octane/air, H_2/air and syngas/air mixtures, respectively. The reduced mechanism also shows good agreement with the LLNL mechanism for the ignition of iso-octane/H_2 and iso-octane/syngas blends. For both mechanisms, the effect of H_2 is relatively small for blends containing less than 50% H_2 by volume, but becomes increasingly significant for higher H_2 fractions. The addition of H_2 increases ignition delay at low temperatures ($T < 900$ K), and decreases it at high temperatures ($T > 1000$ K). For H_2 fractions above 80%, the ignition process is influenced more strongly by the H_2 oxidation chemistry, and does not exhibit the NTC behavior.
3. Another useful interpretation of the present results is that the addition of a relatively small amount of i-C_8H_{18} (a low cetane number fuel) can significantly enhance the ignitability of H_2-air mixtures at temperatures below 1000 K. This temperature range is important for HCCI and PCCI dual fuel engines.
4. The CO addition seems to have a negligible effect on the ignition of iC_8H_{18}/air mixtures, except at low temperatures ($T < 900$ K) and for blends containing more than 90% CO by volume. Thus the ignition behavior of iC_8H_{18}/syngas blends is essentially determined by the iC_8H_{18} and H_2 oxidation chemistries.
5. The sensitivity and reaction path analysis indicates that the iso-octane oxidation is initiated with the production of alkyl radical by H abstraction through reaction R1. Subsequently, for small amounts of H_2 in the blend, the ignition chemistry in the NTC region is characterized by a competition between two oxidation paths represented by reactions R2 and R8, with R8 path dominating, and increasing the ignition delay. As the amount of H_2 in the blend becomes significant, it opens up another path for the consumption of OH through reaction R36 ($H_2 + OH = H_2O + H$). This has the effect of reducing the iC_8H_{18} oxidation rate through its reaction with OH, and thus slowing down the R2 path and increasing the ignition delay. However, at temperatures $T > 1100$ K, the presence of H_2 decreases ignition delay primarily due to reactions R31 ($O_2 + H = OH + O$) and R35 ($H_2O_2 + M = OH + OH + M$).

6. The present work suggests potential new ignition experiments for iso-octane/H_2 and iso-octane/syngas blends. Future experimental studies should also focus on examining the ignition behavior of such blends under spatially non-homogeneous conditions.

Appendix A. Supplementary data

Supplementary data related to this article can be found at http://dx.doi.org/10.1016/j.ijhydene.2013.01.027.

REFERENCES

[1] Maschio G, Lucchesi A, Stoppato G. Production of syngas from biomass. Bioresour Technol 1994;48:119–26.
[2] Goransson K, Soderlind U, He J, Zhang W. Review of syngas production via biomass DFBGs. Renewable Sustainable Energy Rev 2011;15:482–92.
[3] White CM, Steeper RR, Lutz AE. The hydrogen fueled internal combustion engine: a technical review. Int J Hydrogen Energy 2005;31:1292–305.
[4] Das LM. Exhaust emission characterization of hydrogen operated engine system: nature of pollutants and their control techniques. Int J Hydrogen Energy 1991;16:765–75.
[5] Heffel JW. NO_x emission reduction in a hydrogen fueled internal combustion engine at 3000 rpm using exhaust gas recirculation. Int J Hydrogen Energy 2003;28:1285–92.
[6] Guo H, Smallwood GJ, Liu F, Ju Y, Gulder OL. The effect of hydrogen addition on flammability limit and NO_x emission in ultra-lean counterflow CH_4/air premixed flames. Proc Combust Inst 2005;30:303–11.
[7] Yu G, Law CK, Wu CK. Laminar flame speeds of hydrocarbon + air mixtures with hydrogen addition. Combust Flame 1986;63:339–47.
[8] Halter F, Chauveau C, Djebaıli-Chaumeix N, Gokalp I. Characterization of the effects of pressure and hydrogen concentration on laminar burning velocities of methane–hydrogen–air mixtures. Proc Combust Inst 2005; 30:201–8.
[9] Shy SS, Chen YC, Yang CH, Liu CC, Huang CM. Effects of H_2 or CO_2 addition, equivalence ratio, and turbulent straining on turbulent burning velocities for lean premixed methane combustion. Combust Flame 2008;153:510–24.
[10] Naha S, Aggarwal SK. Fuel effects on NO_x emissions in partially premixed flames. Combust Flame 2004;39:90–105.
[11] Naha S, Briones AM, Aggarwal SK. Effect of fuel blends on pollutants emissions in flames. Combust Sci Technol 2005; 177(1):183–220.
[12] Guo H, Neill WS. A numerical study on the effect of hydrogen/reformate gas addition on flame temperature and NO formation in strained methane/air diffusion flames. Combust Flame 2009;156:477–83.
[13] Briones AM, Aggarwal SK, Katta VR. Effects of H_2 enrichment on the propagation characteristics of CH_4/air triple flames. Combust Flame 2008;153:367–83.
[14] Tuncer O, Acharya S, Uhm JH. Dynamics, NO_x and flashback characteristics of confined premixed hydrogen-enriched methane flames. Int J Hydrogen Energy 2009;34:496–506.
[15] Schefer RW. Hydrogen enrichment for improved lean flame stability. Int J Hydrogen Energy 2003;28:1131–41.
[16] Shirk MG, McGuire TP, Neal GL, Haworth DC. Investigation of a hydrogen-assisted combustion system for a light-duty diesel vehicle. Int J Hydrogen Energy 2008;33:7237–44.
[17] Bauer CG, Forest TW. Effect of hydrogen addition on the performance of methane-fueled vehicles. Part I: effect on SI engine performance. Int J Hydrogen Energy 2001;26:55–70.
[18] Bauer CG, Forest TW. Effect of hydrogen addition on performance of methane-fueled vehicles. Part II: driving cycle simulation. Int J Hydrogen Energy 2001;26:71–90.
[19] Nagalingam B, Duebel F, Schmillen K. Performance study using natural gas, hydrogen supplemented natural gas and hydrogen in AVL research engine. Int J Hydrogen Energy 1983;8(9):715–20.
[20] Karim GA, Wierzba I, Al-Alousi Y. Methane-hydrogen mixtures as fuels. Int J Hydrogen Energy 1996;21(7):625–31.
[21] Ma F, Wang Y, Liu H, Li Y, Wang J, Zhao S. Experimental study on thermal efficiency and emission characteristics of a lean burn hydrogen enriched natural gas engine. Int J Hydrogen Energy 2007;32:5067–75.
[22] Ma F, Wang Y, Liu H, Li Y, Wang J, Ding S. Effects of hydrogen addition on cycle-by-cycle variations in a lean burn natural gas spark-ignition engine. Int J Hydrogen Energy 2008;33: 823–31.
[23] Das LM, Gulati R, Gupta PK. A comparative evaluation of the performance characteristics of a spark ignition engine using hydrogen and compressed natural gas as alternative fuels. Int J Hydrogen Energy 2000;25:783–93.
[24] Sher E, Hacohen Y. Measurements and predictions of the fuel consumption and emission of a spark ignition engine fueled with hydrogen-enriched gasoline. J Power Energy 1989;203: 155–9.
[25] Changwei J, Shuofeng W. Effect of hydrogen addition on the idle performance of a spark ignited gasoline engine at stoichiometric condition. Int J Hydrogen Energy 2009;34: 3546–56.
[26] Andrea TD, Henshaw PF, Ting DSK. The addition of hydrogen to a gasoline-fuelled SI engine. Int J Hydrogen Energy 2004;29: 1541–52.
[27] Kahraman E, Ozcanl SC, Ozerdem B. An experimental study on performance and emission characteristics of a hydrogen fuelled spark ignition engine. Int J Hydrogen Energy 2007;32: 2066–72.
[28] Ji C, Wang S. Effect of hydrogen addition on combustion and emissions performance of a spark ignition gasoline engine at lean conditions. Int J Hydrogen Energy 2009;34:7823–34.
[29] Porpatham E, Ramesh A, Nagalingam B. Effect of hydrogen addition on the performance of a biogas fuelled spark ignition engine. Int J Hydrogen Energy 2007;32(12):2057–65.
[30] Schafer F. An investigation of the addition of hydrogen to methanol on the operation of an unthrottled Otto engine. SAE Paper 1981:810776.
[31] Al-Baghdadi MAS. Hydrogen–ethanol blending as an alternative fuel of spark ignition engines. Renewable Energy 2002;28(9):1471–8.
[32] Zhang Y, Huang Z, Wei L, Zhang J, Law CK. Experimental and modeling study on ignition delays of lean mixtures of methane, hydrogen, oxygen, and argon at elevated pressures. Combust Flame 2012;159:918–31.
[33] Huang J, Bushe WK, Hill PG, Munshi SR. Shock initiated ignition in homogeneous methane–hydrogen–air mixtures at high pressure. Int J Chem Kinet 2006;38(4):221–33.
[34] Gersen S, Anikin NB, Mokhova AV, Levinsky HB. Ignition properties of methane/hydrogen mixtures in a rapid compression machine. Int J Hydrogen Energy 2008;33:1957–64.
[35] Aggarwal SK, Awomolo O, Akber K. Ignition characteristics of heptane-hydrogen and heptane-methane fuel blends at elevated pressures. Int J Hydrogen Energy 2011;36:15392–402.
[36] Boehman AL, Le Corre O. Combustion of syngas in internal combustion engines. Combust Sci Tech 2008;180:1193–206.
[37] Azimov U, Tomita E, Kawahara N, Harada Y. Effect of syngas composition on combustion and exhaust emission

characteristics in a pilot-ignited dual-fuel engine operated in PREMIER combustion mode. Int J Hydrogen Energy 2011;36:11985–96.
[38] Jia M, Xie M. A chemical kinetics model of iso-octane oxidation for HCCI engines. Fuel 2006;85:2593–604.
[39] Davidson DF, Gauthier BM, Hanson RK. Shock tube ignition measurements of iso-octane/air and toluene/air at high pressures. Proc Combust Inst 2005;30:1175–82.
[40] Walton SM, He X, Zigler BT, Wooldridge MS, Atreya A. An experimental investigation of iso-octane ignition phenomena. Combust Flame 2007;150:246–62.
[41] Petersen EL, Kalitan DM, Barrett AB, Reehal SC, Mertens JD, Beerer DJ, et al. New syngas/air ignition data at lower temperature and elevated pressure and comparison to current kinetics models. Combust Flame 2007;149:244–7.
[42] Walton SM, He X, Zigler BT, Wooldridge MS. An experimental investigation of the ignition properties of hydrogen and carbon monoxide mixtures for syngas turbine applications. Proc Combust Inst 2007;31:3147–54.
[43] Curran HJ, Gaffuri P, Pitz WJ, Westbrook CK. A comprehensive modeling study of iso-octane oxidation. Combust Flame 2002;129:253–80.
[44] Curran HJ, Pitz WJ, Westbrook CK, Callahan CV, Dryer FL. Oxidation of automotive primary reference fuels at elevated pressures. Proc Combust Inst 1998;27:379–87.
[45] Ó Conaire M, Curran HJ, Simmie JM, Pitz WJ, Charles K, Westbrook CK. A comprehensive modeling study of hydrogen oxidation. Int J Chem Kinet 2004;36:603–22.
[46] Li J, Zhao Z, Kazakov A, Dryer FL. An updated comprehensive kinetic model of hydrogen combustion. Int J Chem Kinet 2004;36:566–75.
[47] Davis SG, Joshi AV, Wang H, Egolfopoulos F. An optimized kinetic model of H_2/CO combustion. Proc Combust Inst 2005;30:1283–92.
[48] https://www-pls.llnl.gov/?url=science_and_technology-chemistry-combustion-iso_octane_version_3.
[49] Dryer FL, Chaos M. Ignition of syngas/air and hydrogen/air mixtures at low temperatures and high pressures: experimental data interpretation and kinetic modeling implications. Combust Flame 2008;152:293–9.
[50] Patel A, Kong SC, Reitz RD. Development and validation of reduced reaction mechanism for HCCI engine simulation. SAE; 2004-01-0558.